

Hyperbolic Neural Networks for Molecular Generation

Eric Qu¹ Dongmian Zou¹

Abstract

With the recent advance of deep learning, neural networks have been extensively used for the task of molecular generation. Many deep generators extract atomic relations from molecular graphs and ignore hierarchical information at both atom and molecule levels. In order to extract such hierarchical information, we propose a novel hyperbolic generative model. Our model contains three parts: first, a fully hyperbolic junction-tree encoder-decoder that embeds the hierarchical information of the molecules in the latent hyperbolic space; second, a latent generative adversarial network for generating the latent embeddings; third, a molecular generator that inherits the decoders from the first part and the latent generator from the second part. We evaluate our model on the ZINC dataset using the MOSES benchmarking platform and achieve competitive results, especially in metrics about structural similarity.

1. Introduction

Data in high dimension often show an underlying geometric structure, which cannot be captured by commonly used deep neural networks which are designed for Euclidean objects such as texts and images. Recently, there is intense interest in learning representations for hierarchical data, which naturally appear in tasks such as word embedding (Wang et al., 2019), graph embedding (Bachmann et al., 2020) and action recognition (Peng et al., 2020). A natural manifold for modeling hyperbolic data is the hyperbolic space, which is a Riemannian manifold with constant negative curvature (Anderson, 2006). In particular, the exponential growth of its radius makes the hyperbolic space has high capacity very suitable for modeling tree-like hierarchical structures.

Recently, hyperbolic spaces have also been used to model molecules (Yu et al., 2020). Learning the structures of molecules is a crucial task, which has important application in drug discovery. Since molecules show a graph struc-

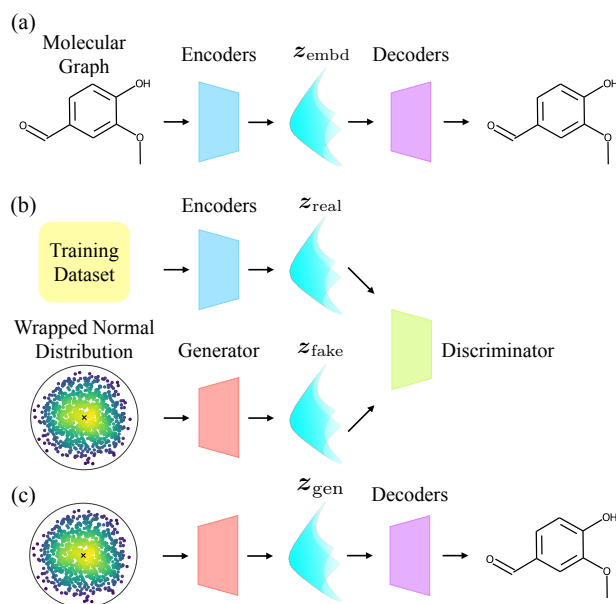


Figure 1. Overview of HJTGAN. (a) The hyperbolic junction tree encoder-decoder (an abbreviated version of Figure 2). (b) The hyperbolic GAN for generating the latent embeddings. The encoders in (b) are identical to (a). (c) The process for sampling molecules. The generator in (c) is identical to (b) and the decoders in (c) are identical to (a).

ture, many works have used graph neural networks to extract their information and trained generators accordingly (Simonovsky & Komodakis, 2018; De Cao & Kipf, 2018; Jin et al., 2018; 2019). However, a graph neural network only concerns the topological representation of molecules as combination of atoms, and the latent space of the representation is still essentially Euclidean. To leverage the structural information of molecules, we represent the molecular data as lying in a latent hyperbolic manifold. Moreover, we use a junction-tree encoder-decoder (Jin et al., 2018; 2019) in the hyperbolic space to represent the structural information of the atoms in each molecule. Putting the atom-level and molecule-level information together, we propose a novel model for molecular generation, which we name as the Hyperbolic Junction-Tree Generative Adversarial Network (HJTGAN). Our model consists of three

¹Division of Natural and Applied Sciences, Duke Kunshan University, Kunshan, Jiangsu, China. Correspondence to: Dongmian Zou <dongmian.zou@duke.edu>.

components. The first component is a hyperbolic junction-tree encoder-decoder. The second component a generative adversarial network (GAN) which inherits the encoders in the first part and uses a wrapped normal distribution input to generate the latent hyperbolic embedding. The third component applies the generator of the GAN and the decoders of the junction-tree encoder-decoder to generate samples of molecular graphs. The whole model of HJTGAN is illustrated in Figure 1.

HJTGAN is a fully hyperbolic model, which means that the operations are completely conducted in the hyperbolic space without going back and forth between the hyperbolic space and the tangent spaces (with the exception when we need to map the input from the Euclidean space or the output to the Euclidean space). In order to achieve that, we work with the Lorentz space and use the linear layers defined by Chen et al. (2021). We also design novel modules including concatenation and split layers, as well as embedding Layers in the Lorentz space. These modules not only guarantee the hidden features are in the hyperbolic space, but also empirically enable stable training for our deep architecture of HJTGAN.

We experimentally illustrate the effectiveness of our neural network using the ZINC dataset on the MOSES benchmark platform (Polykovskiy et al., 2020). Our method achieves state-of-the-art performance in metrics that measure structural similarity. This implies that our hyperbolic approach is effective in learning the underlying manifold structure of the molecular data.

2. Related Work

Machine Learning in Hyperbolic Spaces A central topic in machine learning is to find methods and architectures that incorporate the geometric structure of data (Bronstein et al., 2021). Due to the data representation capacity of the hyperbolic space, many machine learning methods have been designed for hyperbolic data. Such methods include hyperbolic dimensionality reduction (Chami et al., 2021) and kernel hyperbolic methods (Fang et al., 2021). Besides these works, deep neural networks have also been proposed in the hyperbolic domain. One of the earliest such model is the Hyperbolic Neural Network (Ganea et al., 2018) which works with the Poincaré ball model of the hyperbolic space. This is recently refined in the Hyperbolic Neural Network ++ (Shimizu et al., 2021). Another popular choice is to use the Lorentz model of the hyperbolic space. For instance, Chen et al. (2021) works with the Lorentz model and designs a Fully Hyperbolic Neural Network without taking operations in the tangent spaces. Our neural network is also designed in the Lorentz space to enable fully hyperbolic operations.

Hyperbolic Graph Neural Networks Graph neural networks (GNN) are successful models for learning representations of graph data. Recent studies (Boguná et al., 2010; Sala et al., 2018; Krioukov et al., 2010) have found that hyperbolic spaces are suitable for tree-like graphs and a variety of hyperbolic GNNs have been proposed. For instance, Chami et al. (2019); Liu et al. (2019) both perform message passing, the fundamental operation in GNNs, in the tangent space of the hyperbolic space. On the other hand, Dai et al. (2021a); Chen et al. (2021) design fully hyperbolic operations so that message passing can be done completely in the hyperbolic space. Since molecules can be treated as graphs, some of these works (Liu et al., 2019; Dai et al., 2021a) apply hyperbolic GNNs to the task of molecular generation.

Hyperbolic Generative Models Generative neural networks in the Euclidean domain cannot embed information of the hyperbolic geometry. To address that, Nagano et al. (2019) designs a wrapped normal distribution in the hyperbolic space which enables taking gradient and uses it as the latent distribution of a variational autoencoder (VAE). Mathieu et al. (2019) considers both the wrapped normal distribution and maximum entropy normal distribution and uses them to construct an VAE on the Poincaré space. Dai et al. (2021b) also builds a VAE in the Poincaré space, which uses the primal-dual formulation of the Kull-backLeibler (KL) divergence. Other than using VAE, other generation frameworks are also adapted to the hyperbolic space. For instance, Bose et al. (2020) lifts normalizing flows on the tangent plane of the hyperbolic space for generation. Lazcano et al. (2021) uses hyperbolic linear layers in GAN for image generation. Despite the importance of the GAN framework, we are unaware of other hyperbolic GAN models. Our proposed model contains a hyperbolic encoder-decoder to learn the graph-to-graph mapping, as well as a hyperbolic GAN for generating latent embeddings, whose generator uses the wrapped normal distribution as input.

3. Hyperbolic Neural Networks

3.1. Hyperbolic Geometry

Hyperbolic geometry is a special kind of Riemannian geometry with a constant negative curvature (Cannon et al., 1997; Anderson, 2006). There are five models (coordinate systems) of the hyperbolic space: the Lorentz model, the Poincaré ball model, the Hemisphere model, the Klein model, and the Poincaré half-space model. The models are isometric and the relation between their coordinates is surveyed by Dai et al. (2021a). In our model, we work with the Lorentz model since it provides sufficient space for optimization and its numerical stability (Nickel & Kiela, 2018). We describe the fundamental concepts as well as operations used in our neural networks in this section.

The Lorentz Model The Lorentz model $\mathbb{L}_K^n = (\mathcal{L}, \mathbf{g}^K)$ of an n dimensional hyperbolic space with constant negative curvature K is an n -dimensional manifold \mathcal{L} embedded in the $(n + 1)$ -dimensional Minkowski space, together with the Riemannian metric tensor $\mathbf{g}^K = \text{diag}([-1, \mathbf{1}_n^\top])$, where $\mathbf{1}_n$ denotes the n -dimensional vector whose entries are all 1’s. Every point in \mathbb{L}_K^n is represented by $\mathbf{x} = [x_t]$, $x_t > 0$, $\mathbf{x}_s \in \mathbb{R}^n$ and satisfies $\langle \mathbf{x}, \mathbf{x} \rangle_{\mathcal{L}} = 1/K$, where $\langle \cdot, \cdot \rangle_{\mathcal{L}}$ is the Lorentz inner product induced by \mathbf{g}^K :

$$\langle \mathbf{x}, \mathbf{y} \rangle_{\mathcal{L}} := \mathbf{x}^\top \mathbf{g}^K \mathbf{y} = -x_t y_t + \mathbf{x}_s^\top \mathbf{y}_s, \quad \mathbf{x}, \mathbf{y} \in \mathbb{L}_K^n.$$

In the rest of the paper, we will refer to x_t as the “time axis” and \mathbf{x}_s the “spatial axes”, following the convention in special relativity.

Geodesics and Distances Geodesics are shortest paths in a manifold, which generalize the notion of “straight lines” in Euclidean geometry. In particular, the length of a geodesic in \mathbb{L}_K^n (the “distance”) between $\mathbf{x}, \mathbf{y} \in \mathbb{L}_K^n$ is given by

$$d_{\mathcal{L}}(\mathbf{x}, \mathbf{y}) = \frac{1}{\sqrt{-K}} \cosh^{-1}(K \langle \mathbf{x}, \mathbf{y} \rangle_{\mathcal{L}}).$$

Tangent Space For each point $\mathbf{x} \in \mathbb{L}_K^n$, the tangent space at \mathbf{x} is $\mathcal{T}_{\mathbf{x}} \mathbb{L}_K^n := \{\mathbf{y} \in \mathbb{R}^{n+1} \mid \langle \mathbf{y}, \mathbf{x} \rangle_{\mathcal{L}} = 0\}$. It is a first order approximation of the hyperbolic manifold around a point \mathbf{x} and is a subspace of \mathbb{R}^{n+1} . We denote $\|\mathbf{v}\|_{\mathcal{L}} = \sqrt{\langle \mathbf{v}, \mathbf{v} \rangle_{\mathcal{L}}}$ as the norm of $\mathbf{v} \in \mathcal{T}_{\mathbf{x}} \mathbb{L}_K^n$.

Exponential and Logarithmic Maps The exponential and logarithmic maps are maps between hyperbolic spaces and their tangent spaces. For $\mathbf{x}, \mathbf{y} \in \mathbb{L}_K^n$ and $\mathbf{v} \in \mathcal{T}_{\mathbf{x}} \mathbb{L}_K^n$, the exponential map $\exp_{\mathbf{x}}^K(\mathbf{v}) : \mathcal{T}_{\mathbf{x}} \mathbb{L}_K^n \rightarrow \mathbb{L}_K^n$ maps tangent vectors to hyperbolic spaces by assigning \mathbf{v} to the point $\exp_{\mathbf{x}}^K(\mathbf{v}) := \gamma(1)$, where γ is the geodesic satisfying $\gamma(0) = \mathbf{x}$ and $\gamma'(0) = \mathbf{v}$. Specifically,

$$\exp_{\mathbf{x}}^K(\mathbf{v}) = \cosh(\phi) \mathbf{x} + \sinh(\phi) \frac{\mathbf{v}}{\phi}, \quad \phi = \sqrt{-K} \|\mathbf{v}\|_{\mathcal{L}}.$$

The logarithmic map $\log_{\mathbf{x}}^K(\mathbf{y}) : \mathbb{L}_K^n \rightarrow \mathcal{T}_{\mathbf{x}} \mathbb{L}_K^n$ is the inverse map that satisfies $\log_{\mathbf{x}}^K(\exp_{\mathbf{x}}^K(\mathbf{v})) = \mathbf{v}$. Specifically,

$$\log_{\mathbf{x}}^K(\mathbf{y}) = \frac{\cosh^{-1}(\psi)}{\sqrt{\psi^2 - 1}} (\mathbf{y} - \psi \mathbf{x}), \quad \psi = K \langle \mathbf{x}, \mathbf{y} \rangle_{\mathcal{L}}.$$

Parallel Transport For two points $\mathbf{x}, \mathbf{y} \in \mathbb{L}_K^n$, the parallel transport from \mathbf{x} to \mathbf{y} defines a map $\text{PT}_{\mathbf{x} \rightarrow \mathbf{y}}^K$, which “transports” a vector from $\mathcal{T}_{\mathbf{x}} \mathbb{L}_K^n$ to $\mathcal{T}_{\mathbf{y}} \mathbb{L}_K^n$ along the geodesic from \mathbf{x} to \mathbf{y} . Parallel transport preserves the metric, i.e. $\forall \mathbf{u}, \mathbf{v} \in \mathcal{T}_{\mathbf{x}} \mathbb{L}_K^n$, $\langle \text{PT}_{\mathbf{x} \rightarrow \mathbf{y}}^K(\mathbf{v}), \text{PT}_{\mathbf{x} \rightarrow \mathbf{y}}^K(\mathbf{u}) \rangle_{\mathcal{L}} = \langle \mathbf{v}, \mathbf{u} \rangle_{\mathcal{L}}$. In particular, the parallel transport in \mathbb{L}_K^n is given by

$$\text{PT}_{\mathbf{x} \rightarrow \mathbf{y}}^K(\mathbf{v}) = \frac{\langle \mathbf{v}, \mathbf{v} \rangle_{\mathcal{L}}}{-1/K - \langle \mathbf{x}, \mathbf{y} \rangle_{\mathcal{L}}} (\mathbf{x} + \mathbf{y}).$$

Wrapped Normal Distribution The wrapped normal distribution is a hyperbolic distribution whose density can be evaluated analytically and differentiable with respect to the parameters (Nagano et al., 2019). Given $\boldsymbol{\mu} \in \mathbb{L}_K^n$ and $\boldsymbol{\Sigma} \in \mathbb{R}^{n \times n}$, to sample $\mathbf{z} \in \mathbb{L}_K^n$ from the wrapped normal distribution $\mathcal{G}(\boldsymbol{\mu}, \boldsymbol{\Sigma})$, we first sample a vector $\tilde{\mathbf{v}}$ from the Euclidean normal distribution $\mathcal{N}(\mathbf{0}, \boldsymbol{\Sigma})$, then identify $\tilde{\mathbf{v}}$ as an element $\mathbf{v} \in \mathcal{T}_{\mathbf{o}} \mathbb{L}_K^n$ so that $\mathbf{v} = \begin{bmatrix} 0 \\ \tilde{\mathbf{v}} \end{bmatrix}$. We parallel transport this \mathbf{v} to $\mathbf{u} = \text{PT}_{\mathbf{o} \rightarrow \boldsymbol{\mu}}^K(\mathbf{v})$ and then finally map \mathbf{u} to $\mathbf{z} = \exp_{\boldsymbol{\mu}}(\mathbf{u}) \in \mathbb{L}_K^n$.

Centroid The notion of the centroid (also called center of mass) of a set of points is important in formulating attention mechanism and feature aggregation in graph neural networks. This notion is extended to the Lorentz model by Law et al. (2019). With the squared Lorentzian distance defined as $d_{\mathcal{L}}^2(\mathbf{x}, \mathbf{y}) = 2/K - 2\langle \mathbf{x}, \mathbf{y} \rangle_{\mathcal{L}}$, $\mathbf{x}, \mathbf{y} \in \mathbb{L}_K^n$, they define the centroid to be the minimizer that solves $\min_{\boldsymbol{\mu} \in \mathbb{L}_K^n} \sum_{i=1}^N \nu_i d_{\mathcal{L}}^2(\mathbf{x}_i, \boldsymbol{\mu})$ subject to $\mathbf{x}_i \in \mathbb{L}_K^n$, $\nu_i \geq 0$, $\sum_i \nu_i > 0$, $i = 1, \dots, N$. A closed form of the centroid is given by

$$\boldsymbol{\mu} = \text{HCent}(\mathbf{X}, \boldsymbol{\nu}) = \frac{\sum_{i=1}^N \nu_i \mathbf{x}_i}{\sqrt{-K} \left\| \sum_{i=1}^N \nu_i \mathbf{x}_i \right\|_{\mathcal{L}}}, \quad (1)$$

where \mathbf{X} is the collection of \mathbf{x}_i ’s that is represented as a matrix whose i -th row is \mathbf{x}_i .

Lorentz Concatenation and Split Concatenation and split are essential operations in neural networks for feature combination, parallel computation, convolution, etc. However, there is no obvious way of doing them in the hyperbolic space. Shimizu et al. (2021) proposes Poincaré β -concatenation and β -split in the Poincaré model. Specifically, they first use the logarithmic map to lift hyperbolic points to the tangent plane of the origin, which is an Euclidean subspace. Then, they perform Euclidean concatenation and split in this tangent space. Finally, they apply β regularization and apply the exponential map to bring it back to the Poincaré ball.

Since we use the Lorentz model, the above operations are not useful and we need to define concatenation and split in the Lorentz space. Before we introduce our definition, we remark that one could define operations in the tangent space similarly to the Poincaré β -concatenation and β -split. More specifically, if we want to concatenate the input vectors $\{\mathbf{x}_i\}_{i=1}^N$ where each $\mathbf{x}_i \in \mathbb{L}_K^{n_i}$, we could follow a “Lorentz Tangent Concatenation”: first lift each \mathbf{x}_i to $\mathbf{v}_i = \log_{\mathbf{o}}^K(\mathbf{x}_i) = \begin{bmatrix} v_{i_t} \\ \mathbf{v}_{i_s} \end{bmatrix} \in \mathbb{R}^{n_i+1}$, and then perform the Euclidean concatenation to get $\mathbf{v} := (0, \mathbf{v}_{1_s}^\top, \dots, \mathbf{v}_{N_s}^\top)^\top$. Finally, we would get $\mathbf{y} = \exp_{\mathbf{o}}^K(\mathbf{v})$ as a concatenated vector in the hyperbolic space. Similarly, we could perform the “Lorentz Tangent Split” on an input $\mathbf{x}_i \in \mathbb{L}_K^n$ with

split sub-dimensions $\sum_{i=1}^N n_i = n$ to get $\mathbf{v} = \log_o^K(\mathbf{x}) = (0, \mathbf{v}_{1_s}^\top \in \mathbb{R}^{n_1}, \dots, \mathbf{v}_{N_s}^\top \in \mathbb{R}^{n_N})^\top$, $\mathbf{v}_i = [\mathbf{v}_{i_s}^0] \in \mathcal{T}_o \mathbb{L}_K^{n_i}$, and the split vectors $\mathbf{y}_i = \exp_o^K(\mathbf{v}_i)$ successively. Unfortunately, both the Lorentz Tangent Concatenation and the Lorentz Tangent Split are not regularized, which means that the norm of the space dimension will increase after concatenation, and decrease after split. This will make the hidden embeddings numerically unstable. This problem could be solved by adding a hyperbolic linear layer after each concatenation and split, similarly to [Ganea et al. \(2018\)](#), so that we have a trainable scaling factor λ to regularize the norm of the output, but a bigger issue with the Lorentz Tangent Concatenation and Split is that if we use them in a deep neural network, there would be too many exponential and logarithmic maps. Combined with numerous concatenations and splits between time and space dimensions, it suffers from severe precision issue and the gradient easily explodes or vanishes. Since our model contains an autoencoder and a GAN, the structure has to be deep and complicated. Therefore, we abandon the use of the tangent space and propose more direct and numerically friendly operations, which we call the ‘‘Lorentz Direct Concatenation and Split’’ and define as follows.

Given the input vectors $\{\mathbf{x}_i\}_{i=1}^N$ where each $\mathbf{x}_i \in \mathbb{L}_K^{n_i}$ and $M = \sum_{i=1}^N n_i$, the Lorentz Direct Concatenation of $\{\mathbf{x}_i\}_{i=1}^N$ is defined to be a vector $\mathbf{y} \in \mathbb{L}_K^M$ given by

$$\mathbf{y} = \text{HCat}(\{\mathbf{x}_i\}_{i=1}^N) = \begin{bmatrix} \sqrt{\sum_{i=1}^N x_{i_t}^2 + \frac{N-1}{K}} \\ \mathbf{x}_{1_s} \\ \vdots \\ \mathbf{x}_{N_s} \end{bmatrix}. \quad (2)$$

Given an input $\mathbf{x} \in \mathbb{L}_K^n$, the Lorentz Direct Split of \mathbf{x} , with sub-dimensions n_1, \dots, n_N where $\sum_{i=1}^N n_i = n$, will be $\{\mathbf{y}_i\}_{i=1}^N$, where each $\mathbf{y}_i \in \mathbb{L}_K^{n_i}$ is given by first splitting \mathbf{x} in the space dimension as

$$\mathbf{x} = \begin{bmatrix} x_t \\ \mathbf{y}_{1_s} \\ \vdots \\ \mathbf{y}_{N_s} \end{bmatrix},$$

and then calculating the corresponding time dimension as

$$\mathbf{y}_i = \begin{bmatrix} \sqrt{\|\mathbf{y}_{i_s}\|^2 - 1/K} \\ \mathbf{y}_{i_s} \end{bmatrix}. \quad (3)$$

The Lorentz Direct Concatenation and Split allow deep and complex neural network structures and we use them in our model for molecular generation.

3.2. Hyperbolic Layers

In order to take full advantage of the manifold structure, it is advantageous to avoid doing operations in the tangent space.

Therefore, we take a fully hyperbolic approach in our model and use the exponential or logarithmic maps only when we need to take input or output from the Euclidean domain. We describe the main layers that we use in HJTGAN as follows.

3.2.1. HYPERBOLIC LINEAR LAYER

We adopt the fully hyperbolic linear layer from [Chen et al. \(2021\)](#). It is based on a trainable ‘‘linear transformation’’ that maps \mathbb{L}_K^n to \mathbb{L}_K^m . Such linear transformation depends on a matrix $M = \begin{bmatrix} \mathbf{v}^\top \\ \mathbf{W} \end{bmatrix}$, where $\mathbf{v} \in \mathbb{R}^{n+1}$ and $\mathbf{W} \in \mathbb{R}^{m \times (n+1)}$ are trainable parameters. Given an input $\mathbf{x} \in \mathbb{L}_K^n$, the linear transformation produces $f_x(M) \in \mathbb{L}_K^m$, which is given by

$$f_x(M) = f_x \left(\begin{bmatrix} \mathbf{v}^\top \\ \mathbf{W} \end{bmatrix} \right) = \begin{bmatrix} \frac{\sqrt{\|\mathbf{W}\mathbf{x}\|^2 - 1/K}}{\mathbf{v}^\top \mathbf{x}} \mathbf{v}^\top \\ \mathbf{W} \end{bmatrix}.$$

Based on this linear transformation, a hyperbolic linear layer with activation, bias and normalization, as we use in our model, is defined to be

$$\mathbf{y} = \text{HLinear}_{n,m}(\mathbf{x}) = \begin{bmatrix} \sqrt{\|h(\mathbf{W}\mathbf{x}, \mathbf{v})\|^2 - 1/K} \\ h(\mathbf{W}\mathbf{x}, \mathbf{v}) \end{bmatrix}.$$

Here $\mathbf{x} \in \mathbb{L}_K^n$ is the input of the layer and $h(\mathbf{W}\mathbf{x}, \mathbf{v}) = \frac{\lambda \sigma(\mathbf{v}^\top \mathbf{x} + b')}{\|\mathbf{W}\tau(\mathbf{x}) + \mathbf{b}\|} (\mathbf{W}\tau(\mathbf{x}) + \mathbf{b})$, where $\mathbf{v} \in \mathbb{R}^{n+1}$ and $\mathbf{W} \in \mathbb{R}^{m \times (n+1)}$ are trainable weights, \mathbf{b} and b' are trainable biases, σ is the sigmoid function, τ is the activation function, and the trainable parameter $\lambda > 0$ scales the range.

3.2.2. HYPERBOLIC GCN LAYER

The basic structure of graph neural networks consists of feature transformation and node aggregation ([Kipf & Welling, 2017](#)). We adopt the formulation of [Chen et al. \(2021\)](#) to construct hyperbolic layers for graphs. In particular, the feature transformation is realized by the hyperbolic linear layer, and the centroid point following (1) is used as output of node aggregation. Specifically,

$$\begin{aligned} \mathbf{x}_v^{(l)} &= \text{HGCN}(\mathbf{X}^{(l-1)})_v \\ &= \text{HCent}(\{\text{HLinear}_{d_{l-1}, d_l}(\mathbf{x}_u^{(l-1)}) \mid u \in N(v)\}, \mathbf{1}) \end{aligned}$$

where $\mathbf{x}_v^{(l)}$ is the feature of node v in layer l , d_l denotes the dimensionality of layer l , and $N(v)$ is the set of neighbour point of node v . Note that we use a direct aggregation without attention.

3.2.3. HYPERBOLIC CENTROID DISTANCE LAYER

A hyperbolic centroid distance layer aims to map points from \mathbb{L}_K^n to \mathbb{R}^m ([Liu et al., 2019](#)). It is used as the output layer in our model. Given an input $\mathbf{x} \in \mathbb{L}_K^n$, it first initializes m trainable centroids $\{\mathbf{c}_i\}_{i=1}^m \subset \mathbb{L}_K^n$, then produces a distance vector

$$\mathbf{y} = \text{HCDist}_{n,m}(\mathbf{x}) = [d_{\mathcal{L}}(\mathbf{x}, \mathbf{c}_1) \quad \dots \quad d_{\mathcal{L}}(\mathbf{x}, \mathbf{c}_m)]^\top,$$

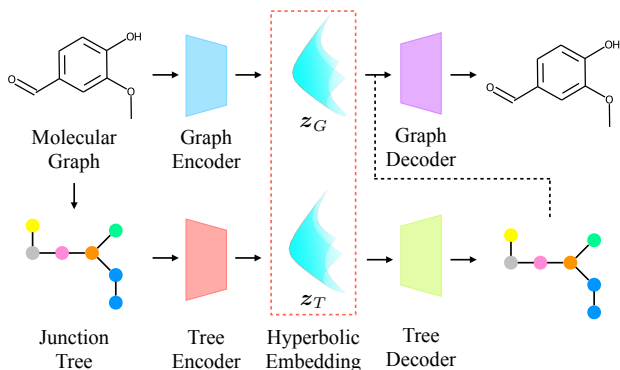


Figure 2. Illustration of the hyperbolic junction tree encoder-decoder used in HJTGAN. The input molecular graph is firstly coarsened into the junction tree. Then both of them are encoded using graph and tree encoders their respective hyperbolic embeddings z_G and z_T . To reconstruct the molecule, we first decode the junction tree from z_T , and then reconstruct the molecular graph using the junction tree and z_G .

This method is more flexible and numerically stable than directly extracting the output from the tangent space \mathbb{R}^{n+1} using the logarithmic map.

3.2.4. HYPERBOLIC EMBEDDING LAYER

In order to map a one-hot vector $\mathbf{x} \in \mathbb{R}^n$ to the hyperbolic space \mathbb{L}_K^m , we design a hyperbolic embedding layer as follows.

We first design a preliminary Euclidean-to-Hyperbolic (E2H) operation that maps a vector $\mathbf{t} \in \mathbb{R}^m$ to \mathbb{L}_K^m . We construct $\mathbf{z} \in \mathcal{T}_o \mathbb{L}_K^m$, where $\mathbf{o} = [\sqrt{-1/K}, 0, \dots, 0]^\top$ is the hyperbolic origin, by $\mathbf{z} = [0, t_1, \dots, t_m]^\top$. Obviously, \mathbf{z} is on the tangent plane since $\langle \mathbf{z}, \mathbf{o} \rangle_{\mathcal{L}} = 0$. Then, we acquire its hyperbolic representation \mathbf{y} by applying an exponential map. Specifically,

$$\mathbf{y} = \text{E2H}_{n,m}(\mathbf{t}) = \exp_{\mathbf{o}}^K \left(\begin{bmatrix} 0 \\ \mathbf{t} \end{bmatrix} \right).$$

To construct a hyperbolic embedding layer for a one-hot vector input, we need more expressivity. Therefore, we first map the input to a hidden embedding $\mathbf{h} = \mathbf{W}\mathbf{x} \in \mathbb{R}^m$ with a trainable embedding matrix $\mathbf{W} \in \mathbb{R}^{n \times m}$. Then, it is mapped to hyperbolic space by the E2H operation defined as above. That is,

$$\mathbf{y} = \text{HEmbed}_{n,m}(\mathbf{x}) = \text{E2H}(\mathbf{W}\mathbf{x}).$$

4. Hyperbolic Junction Tree Encoder-Decoder

HJTGAN uses a fully hyperbolic encoder-decoder for graph-to-graph mapping and feature embedding. We show its basic structure in Figure 2. Following the junction tree variational autoencoder (Jin et al., 2018), we view each molecule as a combination of atom clusters. These clusters form a junction tree, which represents the backbone of the molecule. Within the junction-tree encoder-decoder framework, our model takes a molecule graph as the input, passes the original graph to the graph encoder and feeds the corresponding junction tree to the tree encoder, acquiring latent representation of graph z_G and junction tree z_T , respectively. Then, the junction tree decoder constructs a tree from z_T autoregressively. Finally, the graph decoder recovers the molecule graph using the generated junction tree and z_G . Next, we describe our hyperbolic junction-tree encoder-decoder in detail.

Notation We define the molecular graph as $G = (V_G, E_G)$, where V_G is the set of nodes (atoms) and E_G is the set of edges (bonds). Each node (atom) $v \in V_G$ has a node feature \mathbf{x}_v describing its atom type and properties. The molecular graph is decomposed into a junction tree $T = (V_T, E_T)$ where V_T is the set of atom clusters. We use u, v, w to represent graph nodes and i, j, k to represent tree nodes, respectively. The dimensions of the node features of the graph \mathbf{x}_v and the tree \mathbf{x}_i are denoted by d_{G_0} and d_{T_0} , respectively. The hidden dimensions of graph and tree embeddings are d_G, d_T , respectively.

4.1. Graph and Tree Encoder

We encode the molecular graph G to its hyperbolic embedding using a hyperbolic GCN (Chen et al., 2021). Each node feature \mathbf{x}_v is first mapped to the hyperbolic space via

$$\mathbf{x}_v^{(0)} = \text{E2H}_{d_{G_0}, d_G}(\mathbf{x}_v)$$

and then passed to a hyperbolic GCN with l_G layers

$$\mathbf{x}^{(l)} = \text{HGCN}(\mathbf{x}^{(l-1)}), \quad l = 1, \dots, l_G.$$

Finally, we take the centroid of the embeddings of all vertices to get the hyperbolic embedding z_G of the entire graph,

$$z_G = \text{HCent}(\mathbf{x}^{(l_G)}).$$

The tree decoder is similar with the graph encoder, it encodes the junction tree to hyperbolic embedding z_T with a hyperbolic GCN of depth l_T . The only difference is that its input feature \mathbf{x}_i 's are one-hot vectors representing the atom clusters in the cluster vocabulary. We need to use a hyperbolic embedding layer as the first layer of the network

accordingly. We implement the following successively:

$$\begin{aligned} \mathbf{x}_i^{(0)} &= \text{HEmbed}_{d_{T_0}, d_T}(\mathbf{x}_i), \\ \mathbf{x}^{(l)} &= \text{HGNCN}(\mathbf{x}^{(l-1)}), \quad l = 1, \dots, l_T, \\ \mathbf{z}_T &= \text{HCent}(\mathbf{x}^{(l_T)}). \end{aligned}$$

4.2. Junction Tree Decoder

Following the junction-tree encoder-decoder framework, we generate a junction tree $T = (V_T, E_T)$ using a tree recurrent neural network in a top-down and node-by-node fashion. The generation process resembles a depth-first traversal over the tree T . Starting from the root, at each time step t , the model makes a decision whether to continue generating a child node or backtracking to its parent node. If it decides to generate a new node, it will further predict the cluster label of the child node. It makes these decision based on the messages passed from the neighboring node.

In addition to the fact that our operations are in the hyperbolic space, the main difference between our decoder and the decoder used in JTVAE is that we do not use the gated recurrent unit (GRU) for message passing. The complex structure of GRU will make the training process numerically unstable for our hyperbolic neural network. We simply replace it with a hyperbolic linear layer. Also, JTVAE used ‘‘addition’’ to combine features and make predictions, which, unlike the centroid, does not have a clear definition in the hyperbolic space. Taking this into account, we use the Lorentz Direct Concatenation we defined in (2) to combine features.

Message Passing Let $\tilde{E} = \{(i_1, j_1), \dots, (i_m, j_m)\}$ denote the collection of the edges visited in a depth-first traversal over T , where $m = 2|E_T|$. We store a hyperbolic message \mathbf{h}_{i_t, j_t} for each edge in \tilde{E} . Let \tilde{E}_t be the set of the first t edges in \tilde{E} . Suppose at time step t , the model visit node i_t and it visits node j_t at the next time step. The message \mathbf{h}_{i_t, j_t} is updated using the node feature \mathbf{x}_{i_t} and inward messages \mathbf{h}_{k, i_t} . We first use hyperbolic centroid to gather the inward messages to produce

$$\mathbf{z}_{\text{nei}} = \text{HCent}(\text{HLinear}_{d_T, d_T}(\{\mathbf{h}_{k, i_t}\}_{(k, i_t) \in \tilde{E}, k \neq j_t})),$$

and then map the tree node features to the hyperbolic space to produce

$$\mathbf{z}_{\text{cur}} = \text{HEmbed}_{d_{T_0}, d_T}(\mathbf{x}_{i_t}).$$

Finally, we combine them using the Lorentz Direct Concatenation and pass them through a hyperbolic linear layer to get the message

$$\mathbf{h}_{i_t, j_t} = \text{HLinear}_{2 \times d_T, d_T}(\text{HConcat}(\{\mathbf{z}_{\text{cur}}, \mathbf{z}_{\text{nei}}\})).$$

Topological Prediction At each time step t , the model makes a binary decision on whether to generate a child node, using tree embedding \mathbf{z}_T , node feature \mathbf{x}_{i_t} , and inward messages \mathbf{h}_{k, i_t} using the following layers successively:

$$\begin{aligned} \mathbf{z}_{\text{nei}} &= \text{HCent}(\text{HLinear}_{d_T, d_T}(\{\mathbf{h}_{k, i_t}\}_{(k, i_t) \in \tilde{E}})), \\ \mathbf{z}_{\text{cur}} &= \text{HEmbed}_{d_{T_0}, d_T}(\mathbf{x}_{i_t}), \\ \mathbf{z}_{\text{all}} &= \text{HLinear}_{3 \times d_T, d_T}(\text{HConcat}(\{\mathbf{z}_{\text{cur}}, \mathbf{z}_{\text{nei}}, \mathbf{z}_T\})), \\ \mathbf{p}_t &= \text{Softmax}(\text{HCDist}_{d_T, 2}(\mathbf{z}_{\text{all}})). \end{aligned}$$

Label Prediction If a child node j_t is generated, we use the tree embedding \mathbf{z}_T and the outward message \mathbf{h}_{i_t, j_t} to predict its label. We apply the following two layers successively:

$$\begin{aligned} \mathbf{z}_{\text{all}} &= \text{HLinear}_{2 \times d_T, d_T}(\text{HConcat}(\{\mathbf{h}_{i_t, j_t}, \mathbf{z}_T\})) \\ \mathbf{q}_t &= \text{Softmax}(\text{HCDist}_{d_T, d_{T_0}}(\mathbf{z}_{\text{all}})). \end{aligned}$$

The output \mathbf{q}_t is a distribution over the label vocabulary. When j_t is a root node, its parent i_t is dummy and the message is padded with the origin of the hyperbolic space $\mathbf{h}_{i_t, j_t} = \mathbf{o}$.

Training The topological and label prediction have two induced losses. Suppose $\hat{\mathbf{p}}_t, \hat{\mathbf{q}}_t$ are the the ground truth topological and label value, obtained by doing depth-first traversal on the real junction tree. The decoder minimizes the following cross-entropy loss:

$$L_{\text{topo}} = \sum_{t=1}^m L_{\text{cross}}(\hat{\mathbf{p}}_t, \mathbf{p}_t), \quad L_{\text{label}} = \sum_{t=1}^m L_{\text{cross}}(\hat{\mathbf{q}}_t, \mathbf{q}_t)$$

where L_{cross} is the cross-entropy loss. During the training phase, we use the teacher forcing strategy: after the predictions at each time step, we replace them with the ground truth. This allows the model to learn from the correct history information.

4.3. Graph Decoder

This step assembles a molecule graph given a junction $\hat{T} = (\hat{V}, \hat{E})$ and graph embedding \mathbf{z}_G . Let \mathcal{G}_i be the set of possible candidate subgraphs around tree node i , i.e. the different ways of attaching neighboring clusters to cluster i . We want to design a scoring function for each candidate subgraph $G_j^{(i)} \in \mathcal{G}_i$.

To this end, we first use the hyperbolic GCN and hyperbolic centroid to acquire the hyperbolic embedding $\mathbf{z}_{G_j^{(i)}}$ of each subgraph $G_j^{(i)}$. Specifically,

$$\begin{aligned} \mathbf{x}_v^{(0)} &= \text{E2H}_{d_{G_0}, d_G}(\mathbf{x}_v), \\ \mathbf{x}^{(l)} &= \text{HGNCN}(\mathbf{x}^{(l-1)}), \quad l = 1, \dots, l_G, \\ \mathbf{z}_{G_j^{(i)}} &= \text{HCent}(\mathbf{x}^{(l_G)}). \end{aligned}$$

Then, the embedding of the subgraph is combined with the embedding of the molecular graph \mathbf{z}_G by the Lorentz Direct Concatenation to produce

$$\mathbf{z}_{\text{all}} = \text{HLinear}_{2 \times d_G, d_G}(\text{HCat}(\{\mathbf{z}_{G_j^{(i)}}, \mathbf{z}_G\})),$$

which is then passed to the hyperbolic centroid distance layer to get a score

$$s_j^{(i)} = \text{HCDist}_{d_G, 1}(\mathbf{z}_{\text{all}}) \in \mathbb{R}.$$

Training We define the loss for the graph decoder to be the sum of the cross-entropy losses in each \mathcal{G}_i . Specifically, suppose the correct subgraph is $G_c^{(i)}$,

$$L_{\text{assm}} = \sum_i \left(s_c^{(i)} - \log \sum_{G_j^{(i)} \in \mathcal{G}_i} \exp(s_j^{(i)}) \right)$$

Similar to our junction-tree decoder, we also use teacher forcing for the graph decoder.

5. Hyperbolic Generative Adversarial Networks

In HJTGAN, the generator for the latent embeddings is a hyperbolic GAN. This GAN learns the distribution of the latent embedding of molecules. We remark that the idea of generating latent distributions is also used in the LatentGAN (Prykhodko et al., 2019), with completely different models. Suppose following the steps described in §4, our model has already produced a tree encoder, a graph encoder, a tree decoder and a graph decoder. Using the encoders, we embed the input graphs from the training dataset to the latent hyperbolic space. Our hyperbolic GAN learns this latent distribution. In order to generate novel molecules, we sample from the distribution learned by GAN, and feed it to the tree and graph decoders.

Generator The generator aims to map a wrapped normal distribution $\mathcal{G}(\mathbf{o}, \mathbf{I})$ to a hyperbolic distribution. It contains l_{gen} hyperbolic linear layers. Specifically, we sample $\mathbf{z}^{(0)} \sim \mathcal{G}(\mathbf{o}, \mathbf{I})$ and produce \mathbf{z}_{fake} following

$$\begin{aligned} \mathbf{z}^{(l)} &= \text{HLinear}_{d_{l-1}, d_l}(\mathbf{z}^{(l-1)}), \quad l = 1, \dots, l_{\text{gen}}, \\ \mathbf{z}_{\text{fake}} &= \mathbf{z}^{(l_{\text{gen}})}. \end{aligned}$$

Discriminator The discriminator aims to distinguish between fake and real data. Its output is a score in \mathbb{R} . The discriminator contains l_{dis} hyperbolic linear layers, which are followed by a centroid distance layer. Specifically,

$$\begin{aligned} \mathbf{z}^{(l)} &= \text{HLinear}_{d_{l-1}, d_l}(\mathbf{z}^{(l-1)}), \quad l = 1, \dots, l_{\text{dis}}, \\ s &= \text{HCDist}_{d_{l_{\text{dis}}}, 1}(\mathbf{z}^{(l_{\text{dis}})}). \end{aligned}$$

Training We adopt the framework of Wasserstein GAN (Arjovsky et al., 2017). Wasserstein GAN aims to minimize the Wasserstein-1 (W_1) distance between the generator distribution and data distribution. In our hyperbolic setting, the W_1 distance between two hyperbolic distribution $\mathbb{P}_r, \mathbb{P}_g$ defined on the Lorentz space is

$$W_1(\mathbb{P}_r, \mathbb{P}_g) = \inf_{\gamma \in \Pi(\mathbb{P}_r, \mathbb{P}_g)} \mathbb{E}_{(\mathbf{x}, \mathbf{y}) \sim \gamma} [d_{\mathcal{L}}(\mathbf{x}, \mathbf{y})],$$

where $\Pi(\mathbb{P}_r, \mathbb{P}_g)$ is the set of all joint distributions whose marginals are \mathbb{P}_r and \mathbb{P}_g , respectively. By Kantorovich-Rubinstein duality (Villani, 2009), we have the following more tractable form of W_1 distance

$$W_1(\mathbb{P}_g, \mathbb{P}_r) = \sup_{\|f\|_{\mathcal{L}} \leq 1} \mathbb{E}_{\mathbf{x} \sim \mathbb{P}_r} [f(\mathbf{x})] - \mathbb{E}_{\mathbf{x} \sim \mathbb{P}_g} [f(\mathbf{x})],$$

where the supremum is over all 1-Lipschitz functions $f : \mathbb{L}_K^n \rightarrow \mathbb{R}$. To enforce the 1-Lipschitz constraint on the discriminator, we adopt a penalty term on the gradient following Gulrajani et al. (2017). The loss function is thus

$$\begin{aligned} L_{\text{WGAN}} &= \mathbb{E}_{\hat{\mathbf{x}} \sim \mathbb{P}_g} [D(\hat{\mathbf{x}})] - \mathbb{E}_{\mathbf{x} \sim \mathbb{P}_r} [D(\mathbf{x})] \\ &\quad + \lambda \mathbb{E}_{\hat{\mathbf{x}} \sim \mathbb{P}_{\hat{\mathbf{x}}}} \left[(\|\nabla D(\hat{\mathbf{x}})\|_{\mathcal{L}} - 1)^2 \right], \end{aligned}$$

where $\nabla D(\hat{\mathbf{x}})$ is the Riemannian gradient of $D(\mathbf{x})$ at $\hat{\mathbf{x}}$, \mathbb{P}_g is the generator distribution and \mathbb{P}_r is the data distribution, $\mathbb{P}_{\hat{\mathbf{x}}}$ samples uniformly along the geodesic between pairs of points sampled from \mathbb{P}_g and \mathbb{P}_r . This is because the norm of the Riemannian gradient of the optimal discriminator evaluated at the points is equal to 1 almost surely. The proof is very similar to the Euclidean case (Gulrajani et al., 2017). For completeness we formulate this result in Appendix A.

6. Experiments

Dataset We test our model on the MOSES benchmarking platform (Polykovskiy et al., 2020). The benchmarking dataset is refined from the ZINC dataset (Sterling & Irwin, 2015), which contains about 1.58M training, 176k test, and 176k scaffold test molecules. The molecules in the scaffold test set have different Bemis-Murcko scaffolds (Bemis & Murcko, 1996) than both the training and the test set. They are used to determine whether a model could generate novel scaffolds absent in the training set.

Baselines We compare our model with the following baselines: CharRNN (Segler et al., 2018), VAE (Gómez-Bombarelli et al., 2018; Blaschke et al., 2018), AAE (Kadurin et al., 2017a;b; Polykovskiy et al., 2018), JTVAE (Jin et al., 2018), LatentGAN (Prykhodko et al., 2019), and non-neural models (n-gram generative model, Hidden Markov Model (HMM), combinatorial generator). The

Table 1. Performance of different models in Valid, Unique, IntDiv, Filters, and Novelty metrics. Reported (mean \pm std) over three independent samples.

Model	Valid (\uparrow)	Unique@1k (\uparrow)	Unique@10k (\uparrow)	IntDiv (\uparrow)	IntDiv2 (\uparrow)	Filters (\uparrow)	Novelty (\uparrow)
<i>Train</i>	<i>l</i>	<i>l</i>	<i>l</i>	<i>0.857</i>	<i>0.851</i>	<i>l</i>	<i>l</i>
HMM	0.076 \pm 0.0322	0.623 \pm 0.1224	0.567 \pm 0.1424	0.847 \pm 0.0403	0.810 \pm 0.0507	0.902 \pm 0.0489	0.999\pm0.001
NGram	0.238 \pm 0.0025	0.974 \pm 0.0108	0.922 \pm 0.0019	0.874\pm0.0002	0.864 \pm 0.0002	0.958 \pm 0.001	0.969 \pm 0.001
Combinatorial	1.0\pm0.0	0.998 \pm 0.0015	0.991 \pm 0.0009	0.873 \pm 0.0002	0.867\pm0.0002	0.956 \pm 0.0018	0.988 \pm 0.0008
CharRNN	0.975 \pm 0.0264	1.0\pm0.0	0.999 \pm 0.0003	0.856 \pm 0.0005	0.850 \pm 0.0005	0.994 \pm 0.0034	0.842 \pm 0.0509
AAE	0.937 \pm 0.0341	1.0\pm0.0	0.997 \pm 0.002	0.856 \pm 0.0031	0.850 \pm 0.003	0.996 \pm 0.0006	0.793 \pm 0.0285
VAE	0.977 \pm 0.0012	1.0\pm0.0	0.998 \pm 0.0005	0.856 \pm 0.0004	0.850 \pm 0.0004	0.997\pm0.0002	0.695 \pm 0.0069
LatentGAN	0.897 \pm 0.0029	1.0\pm0.0	0.997 \pm 0.0002	0.857 \pm 0.0007	0.851 \pm 0.0006	0.974 \pm 0.0006	0.914 \pm 0.0058
JTVAE	1.0\pm0.0	1.0\pm0.0	1.0\pm0.0	0.855 \pm 0.0034	0.849 \pm 0.0035	0.976 \pm 0.0016	0.950 \pm 0.0006
HJTGAN (Ours)	1.0\pm0.0	1.0\pm0.0	1.0\pm0.0	0.840 \pm 0.0012	0.833 \pm 0.0015	0.987 \pm 0.0009	0.905 \pm 0.0063

Table 2. Performance of different models in FCD, SNN, Frag, and Scaf metrics. Reported (mean \pm std) over three independent samples.

Model	FCD (\downarrow)		SNN (\uparrow)		Frag (\uparrow)		Scaf (\uparrow)	
	Test	TestSF	Test	TestSF	Test	TestSF	Test	TestSF
<i>Train</i>	<i>0.008</i>	<i>0.476</i>	<i>0.642</i>	<i>0.586</i>	<i>l</i>	<i>0.999</i>	<i>0.991</i>	<i>0</i>
HMM	24.466 \pm 2.5251	25.431 \pm 2.5599	0.388 \pm 0.0107	0.380 \pm 0.0107	0.575 \pm 0.1224	0.568 \pm 0.1218	0.207 \pm 0.0481	0.049 \pm 0.018
NGram	5.507 \pm 0.1027	6.231 \pm 0.0966	0.521 \pm 0.001	0.500 \pm 0.0005	0.985 \pm 0.0012	0.982 \pm 0.0012	0.530 \pm 0.0163	0.098 \pm 0.0142
Combinatorial	4.238 \pm 0.037	4.511 \pm 0.0274	0.451 \pm 0.0003	0.439 \pm 0.0002	0.991 \pm 0.0004	0.990 \pm 0.0003	0.445 \pm 0.0056	0.087 \pm 0.0027
CharRNN	0.073\pm0.0247	0.520\pm0.0379	0.602 \pm 0.0206	0.565 \pm 0.0142	1.0\pm0.0002	0.998 \pm 0.0003	0.924 \pm 0.0058	0.110 \pm 0.0081
AAE	0.556 \pm 0.2033	1.057 \pm 0.2375	0.608 \pm 0.0043	0.568 \pm 0.0045	0.991 \pm 0.0051	0.991 \pm 0.0039	0.902 \pm 0.0375	0.079 \pm 0.009
VAE	0.099 \pm 0.0125	0.567 \pm 0.0338	0.626 \pm 0.0005	0.578 \pm 0.0008	0.999 \pm 0.0001	0.998\pm0.0003	0.939\pm0.0021	0.059 \pm 0.0095
LatentGAN	0.297 \pm 0.0087	0.828 \pm 0.0117	0.537 \pm 0.0004	0.513 \pm 0.0002	0.999 \pm 0.0004	0.997 \pm 0.0007	0.887 \pm 0.0009	0.107 \pm 0.0098
JTVAE	0.395 \pm 0.0234	0.938 \pm 0.0531	0.548 \pm 0.0076	0.519 \pm 0.007	0.997 \pm 0.0003	0.995 \pm 0.0002	0.896 \pm 0.0039	0.101 \pm 0.0105
HJTGAN (Ours)	0.819 \pm 0.0317	1.343 \pm 0.0454	0.631\pm0.0037	0.593\pm0.0023	0.996 \pm 0.0004	0.995 \pm 0.0005	0.874 \pm 0.0024	0.113\pm0.0073

benchmark results are taken from Polykovskiy et al. (2020)¹.

Metrics The models are evaluated using the following metrics. We generate 30,000 molecules which we call the generated set. The generated set is compared with the test set and the scaffold set when evaluating relevant metrics. *Validity* and *Unique*(ness) are the percentage of valid and unique molecules in the generated set, respectively. Internal diversity (*IntDiv*) assesses the chemical diversity within the generated set, which indicates whether the model has mode collapse. *Filters* is the percentage of molecules that passed the filter applied on ZINC. *Novelty* is the fraction of molecules that are not in training set. Fréchet ChemNet Distance (*FCD*) is the difference in the distribution of the last layer of ChemNet. Similarity to a Nearest Neighbor (*SNN*) is the average similarity between generated molecule and its nearest neighbor in the reference set. Fragment similarity (*Frag*) and Scaffold similarity (*Scaf*) are cosine distances between fragment or scaffold frequency vectors of the generated and reference sets, respectively.

Results We describe the detailed settings and hyperparameters in Appendix B. The molecules generated by our model are available at <https://github.com/yhzq/HJTGAN> and we present some examples in Appendix C. The results are presented in Tables 1 and 2.

First of all, our model achieves perfect validity and uniqueness scores, which implies working with the hyperbolic

¹We take the most updated results available from <https://github.com/molecularsets/moses>.

space does not break the graph structures and does not induce mode collapse. Our model significantly outperforms the baseline models in the SNN metric. This means that the molecules generated by our model have a closer similarity to the reference set (Polykovskiy et al., 2020). It implies that our model captures better the underlying manifold structure of the molecules and our hyperbolic latent space is more suitable for embedding molecules than its Euclidean counterparts. Our model also achieves competitive performance in the Scaf metric when the reference set is the scaffold test set. This shows that our model is better in searching on the manifold of scaffolds and can generate novel scaffold.

In most other metrics, our model is on par with the baselines. In particular, in IntDiv, IntDiv2, Filters, Frag, we achieve similar results with JTVAE, which suggests that working in the hyperbolic space does not undermine the expressivity or capacity of the junction-tree framework. Our model is not competitive in the FCD score. We guess the reason is that FCD, as a Wasserstein distance between normal distributions, is intrinsically Euclidean. Our samples are drawn from a hyperbolic latent space, so the activations from the ChemNet, which is also Euclidean, are not very close in distribution to the reference set.

7. Conclusion

In this paper, we propose a fully hyperbolic model for molecular generation. Our model achieves competitive results on the ZINC dataset and in particular significantly outperforms the benchmarks in metrics related to structural similarities. In future work, we will try to generalize our method to other

types of data which have a hyperbolic structure.

Acknowledgement

The authors thank Marcus Werner for helpful discussions. DZ is supported by Kunshan Government Research (KGR) fund.

References

- Anderson, J. W. *Hyperbolic geometry*. Springer Science & Business Media, 2006.
- Arjovsky, M., Chintala, S., and Bottou, L. Wasserstein generative adversarial networks. In *International Conference on Machine Learning*, pp. 214–223. PMLR, 2017.
- Bachmann, G., Bécigneul, G., and Ganea, O. Constant curvature graph convolutional networks. In *International Conference on Machine Learning*, pp. 486–496. PMLR, 2020.
- Bemis, G. W. and Murcko, M. A. The properties of known drugs. 1. molecular frameworks. *Journal of medicinal chemistry*, 39(15):2887–2893, 1996.
- Blaschke, T., Olivecrona, M., Engkvist, O., Bajorath, J., and Chen, H. Application of generative autoencoder in de novo molecular design. *Molecular informatics*, 37(1-2): 1700123, 2018.
- Boguná, M., Papadopoulos, F., and Krioukov, D. Sustaining the internet with hyperbolic mapping. *Nature communications*, 1(1):1–8, 2010.
- Bose, J., Smofsky, A., Liao, R., Panangaden, P., and Hamilton, W. Latent variable modelling with hyperbolic normalizing flows. In *International Conference on Machine Learning*, pp. 1045–1055. PMLR, 2020.
- Bronstein, M. M., Bruna, J., Cohen, T., and Velicković, P. Geometric deep learning: Grids, groups, graphs, geodesics, and gauges. *arXiv preprint arXiv:2104.13478*, 2021.
- Cannon, J. W., Floyd, W. J., Kenyon, R., Parry, W. R., et al. Hyperbolic geometry. *Flavors of geometry*, 31(59-115): 2, 1997.
- Chami, I., Ying, Z., Ré, C., and Leskovec, J. Hyperbolic graph convolutional neural networks. *Advances in neural information processing systems*, 32:4868–4879, 2019.
- Chami, I., Gu, A., Nguyen, D. P., and Ré, C. Horopca: Hyperbolic dimensionality reduction via horospherical projections. In *International Conference on Machine Learning*, pp. 1419–1429. PMLR, 2021.
- Chen, W., Han, X., Lin, Y., Zhao, H., Liu, Z., Li, P., Sun, M., and Zhou, J. Fully hyperbolic neural networks. *arXiv preprint arXiv:2105.14686*, 2021.
- Dai, J., Wu, Y., Gao, Z., and Jia, Y. A hyperbolic-to-hyperbolic graph convolutional network. In *Proceedings of the IEEE/CVF Conference on Computer Vision and Pattern Recognition*, pp. 154–163, 2021a.
- Dai, S., Gan, Z., Cheng, Y., Tao, C., Carin, L., and Liu, J. Apo-vae: Text generation in hyperbolic space. In *Proceedings of the 2021 Conference of the North American Chapter of the Association for Computational Linguistics: Human Language Technologies*, pp. 416–431, 2021b.
- De Cao, N. and Kipf, T. MolGAN: An Implicit Generative Model for Small Molecular Graphs. *ICML 2018 workshop on Theoretical Foundations and Applications of Deep Generative Models*, 2018.
- Fang, P., Harandi, M., and Petersson, L. Kernel methods in hyperbolic spaces. In *Proceedings of the IEEE/CVF International Conference on Computer Vision*, pp. 10665–10674, 2021.
- Ganea, O., Bécigneul, G., and Hofmann, T. Hyperbolic neural networks. *Advances in neural information processing systems*, 31:5345–5355, 2018.
- Gómez-Bombarelli, R., Wei, J. N., Duvenaud, D., Hernández-Lobato, J. M., Sánchez-Lengeling, B., Sheberla, D., Aguilera-Iparraguirre, J., Hirzel, T. D., Adams, R. P., and Aspuru-Guzik, A. Automatic chemical design using a data-driven continuous representation of molecules. *ACS central science*, 4(2):268–276, 2018.
- Gulrajani, I., Ahmed, F., Arjovsky, M., Dumoulin, V., and Courville, A. C. Improved training of wasserstein gans. In Guyon, I., Luxburg, U. V., Bengio, S., Wallach, H., Fergus, R., Vishwanathan, S., and Garnett, R. (eds.), *Advances in Neural Information Processing Systems*, volume 30. Curran Associates, Inc., 2017.
- Jin, W., Barzilay, R., and Jaakkola, T. Junction tree variational autoencoder for molecular graph generation. In *International Conference on Machine Learning*, pp. 2323–2332. PMLR, 2018.
- Jin, W., Yang, K., Barzilay, R., and Jaakkola, T. Learning multimodal graph-to-graph translation for molecule optimization. In *International Conference on Learning Representations*, 2019.
- Kadurin, A., Aliper, A., Kazennov, A., Mamoshina, P., Vanhaelen, Q., Khrabrov, K., and Zhavoronkov, A. The cornucopia of meaningful leads: Applying deep adversarial autoencoders for new molecule development in oncology. *Oncotarget*, 8(7):10883, 2017a.

- Kadurin, A., Nikolenko, S., Khrabrov, K., Aliper, A., and Zhavoronkov, A. drugan: an advanced generative adversarial autoencoder model for de novo generation of new molecules with desired molecular properties in silico. *Molecular pharmaceutics*, 14(9):3098–3104, 2017b.
- Kipf, T. N. and Welling, M. Semi-supervised classification with graph convolutional networks. In *International Conference on Learning Representations (ICLR)*, 2017.
- Kochurov, M., Karimov, R., and Kozlukov, S. Geoopt: Riemannian optimization in PyTorch, 2020.
- Krioukov, D., Papadopoulos, F., Kitsak, M., Vahdat, A., and Boguná, M. Hyperbolic geometry of complex networks. *Physical Review E*, 82(3):036106, 2010.
- Law, M., Liao, R., Snell, J., and Zemel, R. Lorentzian distance learning for hyperbolic representations. In *International Conference on Machine Learning*, pp. 3672–3681. PMLR, 2019.
- Lazcano, D., Franco, N. F., and Creixell, W. HGAN: Hyperbolic generative adversarial network. *IEEE Access*, 9:96309–96320, 2021. doi: 10.1109/ACCESS.2021.3094723.
- Liu, Q., Nickel, M., and Kiela, D. Hyperbolic graph neural networks. *Advances in Neural Information Processing Systems*, 32:8230–8241, 2019.
- Mathieu, E., Le Lan, C., Maddison, C. J., Tomioka, R., and Teh, Y. W. Continuous hierarchical representations with poincaré variational auto-encoders. In Wallach, H., Larochelle, H., Beygelzimer, A., d'Alché-Buc, F., Fox, E., and Garnett, R. (eds.), *Advances in Neural Information Processing Systems*, volume 32. Curran Associates, Inc., 2019.
- Nagano, Y., Yamaguchi, S., Fujita, Y., and Koyama, M. A wrapped normal distribution on hyperbolic space for gradient-based learning. In *International Conference on Machine Learning*, pp. 4693–4702. PMLR, 2019.
- Nickel, M. and Kiela, D. Learning continuous hierarchies in the lorentz model of hyperbolic geometry. In *International Conference on Machine Learning*, pp. 3779–3788. PMLR, 2018.
- Peng, W., Shi, J., Xia, Z., and Zhao, G. Mix dimension in poincaré geometry for 3d skeleton-based action recognition. In *Proceedings of the 28th ACM International Conference on Multimedia*, pp. 1432–1440, 2020.
- Polykovskiy, D., Zhebrak, A., Vetrov, D., Ivanenkov, Y., Aladinskiy, V., Mamoshina, P., Bozdaganyan, M., Aliper, A., Zhavoronkov, A., and Kadurin, A. Entangled conditional adversarial autoencoder for de novo drug discovery. *Molecular pharmaceutics*, 15(10):4398–4405, 2018.
- Polykovskiy, D., Zhebrak, A., Sanchez-Lengeling, B., Golo- vanov, S., Tatanov, O., Belyaev, S., Kurbanov, R., Artamonov, A., Aladinskiy, V., Veselov, M., et al. Molecular sets (moses): a benchmarking platform for molecular generation models. *Frontiers in pharmacology*, 11:1931, 2020.
- Prykhodko, O., Johansson, S. V., Kotsias, P.-C., Arús-Pous, J., Bjerrum, E. J., Engkvist, O., and Chen, H. A de novo molecular generation method using latent vector based generative adversarial network. *Journal of Cheminformatics*, 11(1):1–13, 2019.
- Sala, F., De Sa, C., Gu, A., and Ré, C. Representation tradeoffs for hyperbolic embeddings. In *International conference on machine learning*, pp. 4460–4469. PMLR, 2018.
- Segler, M. H. S., Kogej, T., Tyrchan, C., and Waller, M. P. Generating focused molecule libraries for drug discovery with recurrent neural networks. *ACS Central Science*, 4(1):120–131, 2018. doi: 10.1021/acscentsci.7b00512.
- Shimizu, R., Mukuta, Y., and Harada, T. Hyperbolic neural networks++. In *International Conference on Learning Representations*, 2021.
- Simonovsky, M. and Komodakis, N. GraphVAE: Towards generation of small graphs using variational autoencoders. In *International conference on artificial neural networks*, pp. 412–422. Springer, 2018.
- Sterling, T. and Irwin, J. J. Zinc 15 – ligand discovery for everyone. *Journal of Chemical Information and Modeling*, 55(11):2324–2337, 2015. doi: 10.1021/acs.jcim.5b00559. PMID: 26479676.
- Villani, C. *Optimal transport: old and new*, volume 338. Springer, 2009.
- Wang, X., Zhang, Y., and Shi, C. Hyperbolic heterogeneous information network embedding. In *Proceedings of the AAAI conference on artificial intelligence*, volume 33, pp. 5337–5344, 2019.
- Yu, K., Visweswaran, S., and Batmanghelich, K. Semi-supervised hierarchical drug embedding in hyperbolic space. *Journal of chemical information and modeling*, 60(12):5647–5657, 2020.

A. Validation of the Hyperbolic Wasserstein GAN Formulation

Proposition A.1. Let \mathbb{P}_r and \mathbb{P}_g be two distribution in the compact space \mathbb{L}_K^n . Let f^* be an optimal solution of

$$\max_{\|f\|_{\mathcal{L}} \leq 1} \mathbb{E}_{\mathbf{y} \sim \mathbb{P}_r}[f(\mathbf{y})] - \mathbb{E}_{\mathbf{x} \sim \mathbb{P}_g}[f(\mathbf{x})],$$

where $\mathbf{x}, \mathbf{y} \in \mathbb{L}_K^n$. Let π be the optimal coupling between \mathbb{P}_r and \mathbb{P}_g that minimizes

$$W(\mathbb{P}_r, \mathbb{P}_g) = \inf_{\pi \in \Pi(\mathbb{P}_r, \mathbb{P}_g)} \mathbb{E}_{(\mathbf{x}, \mathbf{y}) \sim \pi}[d_{\mathcal{L}}(\mathbf{x}, \mathbf{y})],$$

where $\Pi(\mathbb{P}_r, \mathbb{P}_g)$ is the set of joint distributions $\pi(\mathbf{x}, \mathbf{y})$ whose marginals are \mathbb{P}_r and \mathbb{P}_g , respectively. Let $\gamma(t), 0 \leq t \leq 1$ be the geodesic between \mathbf{x} and \mathbf{y} , such that

$$\begin{aligned} \gamma(0) &= \mathbf{x} \\ \gamma(1) &= \mathbf{y} \\ \gamma'(t) &= \mathbf{v}_t \\ \|\mathbf{v}_t\|_{\mathcal{L}} &= d_{\mathcal{L}}(\mathbf{x}, \mathbf{y}) \end{aligned}$$

where $\mathbf{v}_t \in \mathcal{T}\mathbb{L}_K^n$. Let $\mathbf{x}_t = \gamma(t)$. If f^* is differentiable and $\pi(\mathbf{x} = \mathbf{y}) = 0$, then it holds that

$$\mathbb{P}_{(\mathbf{x}, \mathbf{y}) \sim \pi} \left[\nabla f^*(\mathbf{x}_t) = \frac{\mathbf{v}_t}{d_{\mathcal{L}}(\mathbf{x}, \mathbf{y})} \right] = 1$$

Proof. For the optimal solution f^* , we have

$$\mathbb{P}_{(\mathbf{x}, \mathbf{y}) \sim \pi} [f^*(\mathbf{y}) - f^*(\mathbf{x}) = d_{\mathcal{L}}(\mathbf{y}, \mathbf{x})] = 1.$$

Let $\psi(t) = f^*(\mathbf{x}_t) - f^*(\mathbf{x})$, $0 \leq t, t' \leq 1$. Following [Gulrajani et al. \(2017\)](#), it is clear that ψ is $d_{\mathcal{L}}(\mathbf{x}, \mathbf{y})$ -Lipschitz, and $f^*(\mathbf{x}_t) - f^*(\mathbf{x}) = \psi(t) = td_{\mathcal{L}}(\mathbf{x}, \mathbf{y})$, $f^*(\mathbf{x}_t) = f^*(\mathbf{x}) + td_{\mathcal{L}}(\mathbf{x}, \mathbf{y}) = f^*(\mathbf{x}) + t\|\mathbf{v}_t\|_{\mathcal{L}}$.

Let $\mathbf{u}_t = \frac{\mathbf{v}_t}{d_{\mathcal{L}}(\mathbf{x}, \mathbf{y})} \in \mathcal{T}\mathbb{L}_K^n$ be the unit speed directional vector of the geodesic at point \mathbf{x}_t . Let $\alpha : [-1, 1] \rightarrow \mathbb{L}_K^n$ be a differentiable curve with $\alpha(0) = \mathbf{x}_t$ and $\alpha'(0) = \mathbf{u}_t$. Note that $\gamma'(t) = d_{\mathcal{L}}(\mathbf{x}, \mathbf{y})\alpha'(0)$. Therefore,

$$\lim_{h \rightarrow 0} \alpha(h) = \lim_{h \rightarrow 0} \gamma \left(t + \frac{h}{d_{\mathcal{L}}(\mathbf{x}, \mathbf{y})} \right) = \lim_{h \rightarrow 0} \mathbf{x}_{t + \frac{h}{d_{\mathcal{L}}(\mathbf{x}, \mathbf{y})}}$$

The directional derivative can be thus calculated as

$$\begin{aligned} \nabla_{\mathbf{u}_t} f^*(\mathbf{x}_t) &= \left. \frac{d}{d\tau} f^*(\alpha(\tau)) \right|_{\tau=0} = \lim_{h \rightarrow 0} \frac{f^*(\alpha(h)) - f^*(\alpha(0))}{h} \\ &= \lim_{h \rightarrow 0} \frac{f^* \left(\mathbf{x}_{t + \frac{h}{d_{\mathcal{L}}(\mathbf{x}, \mathbf{y})}} \right) - f^*(\mathbf{x}_t)}{h} \\ &= \lim_{h \rightarrow 0} \frac{f^*(\mathbf{x}) + (t + \frac{h}{d_{\mathcal{L}}(\mathbf{x}, \mathbf{y})})d_{\mathcal{L}}(\mathbf{x}, \mathbf{y}) - f^*(\mathbf{x}) - td_{\mathcal{L}}(\mathbf{x}, \mathbf{y})}{h} \\ &= \lim_{h \rightarrow 0} \frac{h}{h} = 1. \end{aligned}$$

Since f^* is 1-Lipschitz, we have $\|\nabla f^*(\mathbf{x}_t)\|_{\mathcal{L}} \leq 1$. This implies

$$\begin{aligned} 1 &\geq \|\nabla f^*(\mathbf{x})\|_{\mathcal{L}}^2 \\ &= \langle \mathbf{u}_t, \nabla f^*(\mathbf{x}_t) \rangle_{\mathcal{L}}^2 + \|\nabla f^*(\mathbf{x}_t) - \langle \mathbf{u}_t, \nabla f^*(\mathbf{x}_t) \rangle_{\mathcal{L}} \mathbf{u}_t\|_{\mathcal{L}}^2 \\ &= |\nabla_{\mathbf{u}_t} f^*(\mathbf{x}_t)|^2 + \|\nabla f^*(\mathbf{x}_t) - \mathbf{u}_t \nabla_{\mathbf{u}_t} f^*(\mathbf{x}_t)\|_{\mathcal{L}}^2 \\ &= 1 + \|\nabla f^*(\mathbf{x}_t) - \mathbf{u}_t\|_{\mathcal{L}}^2 \geq 1. \end{aligned}$$

Therefore, we have $1 = 1 + \|\nabla f^*(\mathbf{x}_t) - \mathbf{u}_t\|_{\mathcal{L}}^2$, $\nabla f^*(\mathbf{x}_t) = \mathbf{u}_t$. This yields $\nabla f^*(\mathbf{x}_t) = \frac{\mathbf{v}_t}{d_{\mathcal{L}}(\mathbf{x}, \mathbf{y})}$.

□

B. Experiment Details

We describe the detailed architecture and settings for HJTGAN used in our experiments. The generated molecules we use for test are available at <https://github.com/yhzq/HJTGAN>. We plan to release our code in the same GitHub page.

B.1. Optimization

We use the Geopt package (Kochurov et al., 2020) for Riemannian optimization. In particular, we use the Riemannian Adam function for gradient descent. We also use Geopt for initializing the weights in all hyperbolic linear layers of our model with the wrapped normal distribution.

B.2. Architecture Details

B.2.1. HYPERBOLIC JUNCTION TREE ENCODER-DECODER

Graph Encoder

- Input: graph node features dimension: 35
- Map features to hyperbolic space: $\mathbb{R}^{35} \rightarrow \mathbb{L}_K^{35}$
- Hyperbolic GCN layers:
 - Input dimension: 35
 - Hidden dimension: 256
 - Depth: 4
 - Output dimension: 256
- Hyperbolic centroid on all vertices
- Output: graph embedding in \mathbb{L}_K^{256}

Tree Encoder

- Input: junction tree features dimension 828
- Hyperbolic embedding layer: $\mathbb{R}^{828} \rightarrow \mathbb{L}_K^{256}$
- Hyperbolic GCN layers:
 - Input dimension: 256
 - Hidden dimension: 256
 - Depth: 4
 - Output dimension: 256
- Hyperbolic centroid on all vertices
- Output: tree embedding in \mathbb{L}_K^{256}

Tree Decoder

- Input: tree embedding in \mathbb{L}_K^{256}
- Message passing RNN:
 - Input: node feature of current tree node, inward messages
 - Hyperbolic linear layer on inward messages: $\mathbb{L}_K^{256} \rightarrow \mathbb{L}_K^{256}$
 - Hyperbolic centroid on inward messages

Hyperbolic Neural Networks for Molecular Generation

- Hyperbolic embedding layer on node feature: $\mathbb{R}^{828} \rightarrow \mathbb{L}_K^{256}$
- Lorentz Direct concatenation on node feature and inward message: $\mathbb{L}_K^{256} \rightarrow \mathbb{L}_K^{512}$
- Hyperbolic linear layer: $\mathbb{L}_K^{512} \rightarrow \mathbb{L}_K^{256}$
- Output dimension: 256
- Topological Prediction:
 - Input: tree embedding, node feature of current tree node, inward messages
 - Hyperbolic linear layer on inward messages: $\mathbb{L}_K^{256} \rightarrow \mathbb{L}_K^{256}$
 - Hyperbolic centroid on inward messages
 - Hyperbolic embedding layer on tree feature: $\mathbb{R}^{828} \rightarrow \mathbb{L}_K^{256}$
 - Lorentz Direct concatenation on node feature, inward message, and tree embedding: $\mathbb{L}_K^{256} \rightarrow \mathbb{L}_K^{768}$
 - Hyperbolic linear layer: $\mathbb{L}_K^{768} \rightarrow \mathbb{L}_K^{256}$
 - Hyperbolic centroid distance layer: $\mathbb{L}_K^{256} \rightarrow \mathbb{R}^2$
 - Softmax on output
 - Output dimension: 2
- Label Prediction:
 - Input: tree embedding, outward messages
 - Lorentz Direct concatenation on outward message, and tree feature: $\mathbb{L}_K^{256} \rightarrow \mathbb{L}_K^{512}$
 - Hyperbolic linear layer: $\mathbb{L}_K^{512} \rightarrow \mathbb{L}_K^{256}$
 - Hyperbolic centroid distance layer: $\mathbb{L}_K^{256} \rightarrow \mathbb{R}^{828}$
 - Softmax on output
 - Output dimension: 828
- Output: junction tree

Graph Decoder

- Input: junction tree, tree message, and graph embedding
- Construction candidate subgraphs
- Hyperbolic graph convolution layers on all subgraphs:
 - Input dimension: 256
 - Hidden dimension: 256
 - Depth: 4
 - Output dimension: 256
- Hyperbolic centroid on vertices of all subgraphs
- Lorentz Direct concatenation on subgraph embedding and graph embedding: $\mathbb{L}_K^{256} \rightarrow \mathbb{L}_K^{512}$
- Hyperbolic linear layer: $\mathbb{L}_K^{512} \rightarrow \mathbb{L}_K^{256}$
- Hyperbolic centroid distance layer: $\mathbb{L}_K^{256} \rightarrow \mathbb{R}$
- Use subgraph score to construct molecular graph
- Output: molecular graph

Hyperparameters

- Manifold curvature: $K = -1.0$
- For all hyperbolic linear layers:
 - Dropout: 0.0
 - Use bias: True
- Optimizer: Riemannian Adam ($\beta_1 = 0.0, \beta_2 = 0.999$)
- Learning rate: $5e-4$
- Learning rate scheduler: StepLR (step = 20000, $\gamma = 0.5$)
- Batch size: 32
- Number of epochs: 20

B.2.2. HYPERBOLIC GENERATIVE ADVERSARIAL NETWORK

Generator

- Input: points sampled from wrapped normal distribution $\mathcal{G}(\mathbf{o}, 1)$ in \mathbb{L}_K^{128}
- Hyperbolic linear layers for graph embedding:
 - Input dimension: 128
 - Hidden dimension: 256
 - Depth: 3
 - Output dimension: 256
- Hyperbolic linear layers for tree embedding:
 - Input dimension: 128
 - Hidden dimension: 256
 - Depth: 3
 - Output dimension: 256
- Output: graph embedding and tree embedding in \mathbb{L}_K^{128}

Discriminator

- Input: graph embedding and tree embedding in \mathbb{L}_K^{128}
- Hyperbolic linear layers for graph embedding:
 - Input dimension: 256
 - Hidden dimension: 256
 - Depth: 2
 - Output dimension: 256
- Hyperbolic linear layers for tree embedding:
 - Input dimension: 256
 - Hidden dimension: 256
 - Depth: 2
 - Output dimension: 256

- Lorentz Direct concatenation on graph embedding and tree embedding: $\mathbb{L}_K^{256} \rightarrow \mathbb{L}_K^{512}$
- Hyperbolic linear layer: $\mathbb{L}_K^{512} \rightarrow \mathbb{L}_K^{256}$
- Hyperbolic centroid distance layer: $\mathbb{L}_K^{256} \rightarrow \mathbb{R}$
- Output: score in \mathbb{R}

Hyperparameters

- Manifold curvature: $K = -1.0$
- For all hyperbolic linear layers:
 - Dropout: 0.1
 - Use bias: True
- Optimizer: Riemannian Adam ($\beta_1 = 0, \beta_2 = 0.9$)
- Learning Rate: 1e-4
- Batch size: 64
- Number of epochs: 20

B.2.3. ENVIRONMENTS

- GPU: RTX 3090
- CUDA Version: 11.1
- PyTorch Version: 1.9.0
- RDKit Version: 2020.09.1.0

C. Molecule Examples

We show some examples of the molecules generated by HJTGAN. This is a subset of the examples available at <https://github.com/yhzq/HJTGAN>.

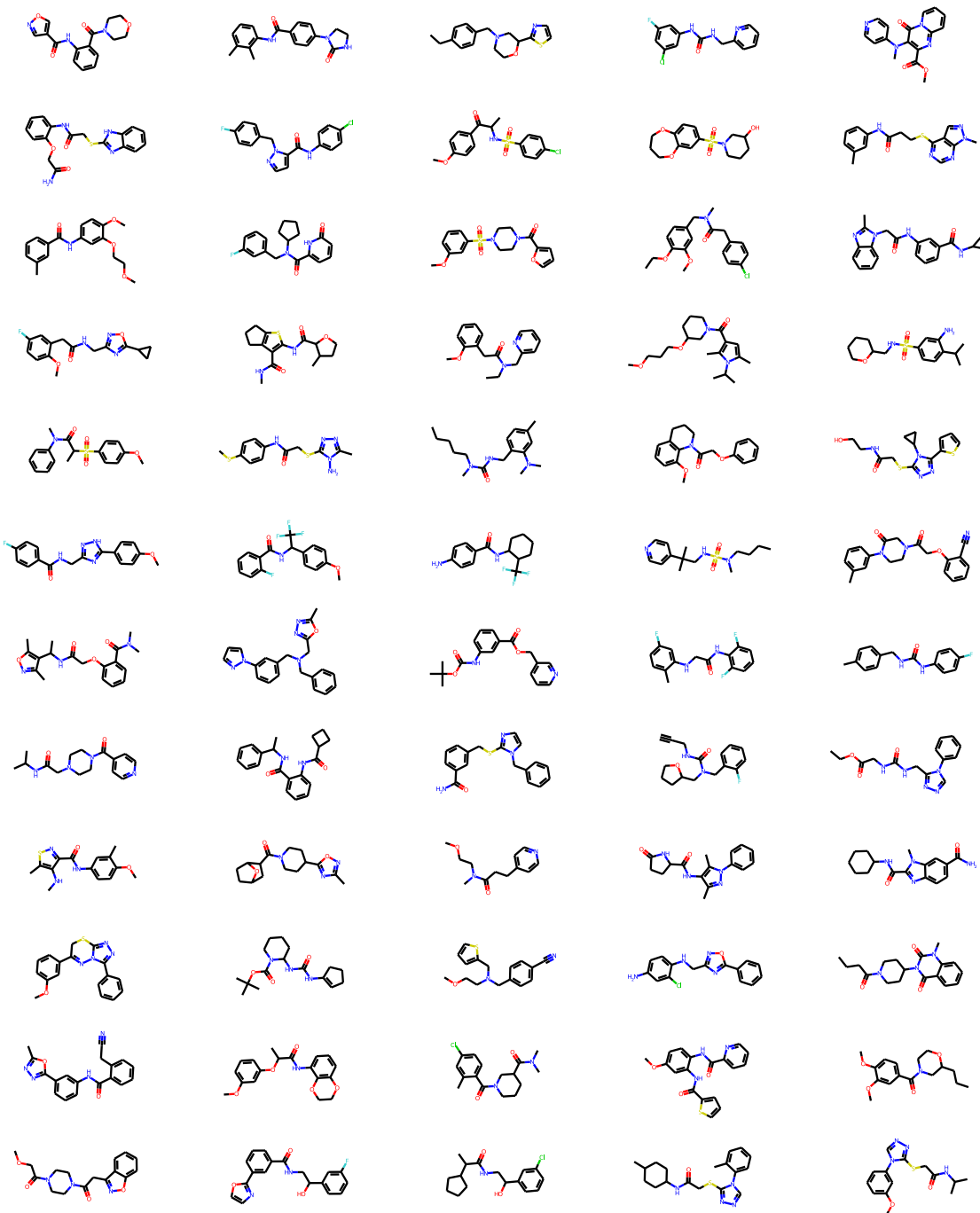


Figure 3. Molecule examples generated by our model.